Available online at www.sciencedirect.com
SCIENCE DIRECT®
PERGAMON
Computers and Structures 81 (2003) 2021–2027
Computers & Structures
www.elsevier.com/locate/compstruc

Micromechanics of braided composites via multivariable FEM

Huiyu Sun [a,*], Shenglin Di [b], Nong Zhang [b], Ning Pan [a], Changchun Wu [c]

[a] Department of Biological and Agricultural Engineering, University of California, Davis, CA 95616, USA
[b] Faculty of Engineering, University of Technology, Sydney, NSW 2007, Australia
[c] Department of Modern Mechanics, University of Science and Technology of China, Anhui 230027, China

Received 14 May 2002; accepted 17 March 2003

Abstract

A new method for micromechanical properties of three-dimensionally braided composite materials via homogenization theory and incompatible multivariable FEM is proposed in this paper. An incompatible displacement element and a hybrid stress element are developed to model the effective mechanical properties of three-dimensional textile composites. Some illustrative applications are presented for a typical class of four-step braided composites. Results of the hybrid stress element approach compare more favorably with the experimental data than other numerical methods widely used.

Keywords: Three-dimensionally braided composites; Multivariable finite element method; Homogenization theory; Incompatible element; Hybrid element; Effective mechanical properties

1. Introduction

Earlier researches in constitutive characteristics of 3-D braided composites were carried out based on a large number of assumptions in simplifying the analysis, such as the widely used isostrain or isostress assumptions regarding the distribution of strain or stress in a loaded structure [1]. When the strain distribution between various laminate subsystems is assumed to be uniform, the isostrain model is obtained [2,3]. On the other hand, if the stress distribution between various laminate subsystems is assumed to be uniform, the isostress model is obtained. A direct consequence of the assumptions in the isostrain and isostress models is the violation of equilibrium and compatibility conditions, respectively, between the laminate subsystems in the unit cell. For instance, for composites with a significant fraction of the fibers that orient at a low angle (15–30°) from the loading direction, the isostrain model predictions deviated significantly from the experimental measurements [3].

Finite element analysis is a useful and versatile approach employed by many researchers to predict material mechanical properties. One of such approaches termed hybrid stress element [4] was proposed by Pian in 1964, and the theory and application of the hybrid elements have since been greatly developed and improved. An optimizing condition for hybrid elements was offered, and a new approach for developing optimal stress patterns was presented. With this approach, a more general resultant element by Wu and Bufler [5] was established without any treatment of perturbations. The optimized hybrid model shows a superior numerical behavior. This can be verified by some benchmark problems in comparison with analytical solutions, for example, cantilevers under loads at ends, hollow spheres with thick walls under inner pressures, etc. [6].

On the other hand, for heterogeneous materials like the textile composites, mathematical homogenization theory [7–10] seems to be the most suitable approach to estimate the macro-level effective elastic properties based on the microstructures. This theory in essence can be viewed as a kind of singular perturbation methods

* Corresponding author. Tel.: +1-530-752-8984; fax: +1-530-752-7584.
E-mail address: hsun@ucdavis.edu (H. Sun).

0045-7949/03/$ - see front matter
doi:10.1016/S0045-7949(03)00228-1

suitable for problems with boundary layers [11] that exist at regions near the interfaces of different phases in a heterogeneous medium. Increasingly the theory has been employed in conjunction with the finite element method for the solution of heterogeneous materials [12–22]. However, since the displacement field was interpolated with the isoparametric elements in this approach, the selective reduced integration has to be used to avoid locking [22]. Furthermore, the Voronoi cell finite element method [15,16] is proposed for analyzing microstructures which consist of random dispersions of second phase inclusions in the matrix.

In order to overcome the intrinsic deficiency of the isoparametric finite element treatment, the incompatible element and hybrid element are constructed and applied to the homogenization theory to model the representative unit cell of 3-D braided fabric reinforced composites in this paper.

2. Asymptotic expansion homogenization

We look for an asymptotic expansion of the displacement u_i^ε as follows [22]:

$$u_i^\varepsilon(x) = u_i^0(x,y) + \varepsilon u_i^1(x,y) + \varepsilon^2 u_i^2(x,y) + \cdots \tag{1}$$

where the functions $u_i^0, u_i^1, u_i^2, \ldots$ are Y-periodic with respect to y. The strain and stress can be expanded as

$$e_{ij}(u_i^\varepsilon) = \varepsilon^{-1} e_{ij}^{(-1)} + e_{ij}^{(0)} + \varepsilon e_{ij}^{(1)} + \cdots \tag{2}$$

$$\sigma_{ij}^\varepsilon = \varepsilon^{-1}\sigma_{ij}^{(-1)} + \sigma_{ij}^{(0)} + \varepsilon\sigma_{ij}^{(1)} + \cdots \tag{3}$$

Inserting Eq. (3) into the equilibrium equation, the following equation is deduced since the terms prior to ε^i should be zeros:

$$\frac{\partial}{\partial y_j}[C_{ijkl} e_{ykl}(u_i^{(1)})] = -\frac{\partial C_{ijkl}}{\partial y_j} e_{xkl}(u_i^{(0)}) \tag{4}$$

where

$$\begin{aligned} e_{xij}(u_i^{(0)}) &= \frac{1}{2}\left(\frac{\partial u_i^{(0)}}{\partial x_j} + \frac{\partial u_j^{(0)}}{\partial x_i}\right) \\ e_{yij}(u_i^{(1)}) &= \frac{1}{2}\left(\frac{\partial u_i^{(1)}}{\partial y_j} + \frac{\partial u_j^{(1)}}{\partial y_i}\right) \end{aligned} \tag{5}$$

From the RHS of Eq. (4), $u_i^{(1)}$ may be written as

$$u_i^{(1)}(x,y) = \chi_i^{kl}(y) e_{xkl}(u_i^{(0)}(x)) \tag{6}$$

where $\chi_i^{kl}(y)$ is a Y-periodic function defined in the unit cell Y. If ε tends to be zero, the first two terms are considered in the formula (3). The stress in Ω^ε is

$$\sigma_{ij}^\varepsilon = \sigma_{ij}^{(0)} = C_{ijmn}[T_{mn}^{kl} + e_{ymn}(\chi_i^{kl})] e_{xkl}(u_i^{(0)}) \tag{7}$$

The average of $\sigma_{ij}^{(0)}$ in the domain Y is written as

$$\langle \sigma_{ij}^{(0)} \rangle = C_{ijkl}^H e_{xkl}(u_i^{(0)}) \tag{8}$$

where

$$C_{ijkl}^H = \frac{1}{|Y|}\int_Y C_{ijmn}[T_{mn}^{kl} + e_{ymn}(\chi_i^{kl})]\,\mathrm{d}Y \tag{9}$$

The elastic constant C_{ijkl}^H defined above is independent of y. It is called the homogenized equivalent elastic constant.

3. Finite element method implementation

To obtain the homogenized elastic constant, it is necessary to solve for χ_i^{kl} satisfying Eq. (4), i.e.,

$$\frac{\partial}{\partial y_j}[C_{ijkl} e_{ykl}(\chi_i^{kl})] + \frac{\partial}{\partial y_j}(C_{ijkl}) = 0 \tag{10}$$

It is evident that χ_i^{kl} is the generalized displacement, and $\frac{\partial}{\partial y_j}(C_{ijkl})$ is the generalized force. As

$$\int_Y \frac{\partial}{\partial y_j}[C_{ijkl} e_{ykl}(\chi_i^{kl}) + C_{ijkl}]\varphi\,\mathrm{d}Y = 0 \quad \forall \varphi \in \Omega \tag{11}$$

Use of the divergence theorem gives

$$\int_Y C_{ijkl} e_{ykl}(\chi_i^{kl}) e_{ij}(\varphi)\,\mathrm{d}Y = -\int_Y C_{ijkl} e_{ij}(\varphi)\,\mathrm{d}Y \tag{12}$$

The unit cell of three-dimensionally braided composite materials is idealized as shown in Fig. 1. It is meshed by the hexahedral elements with eight corner nodes. This kind of element, referred to as multiphase element, may comprise more than one kind of materials.

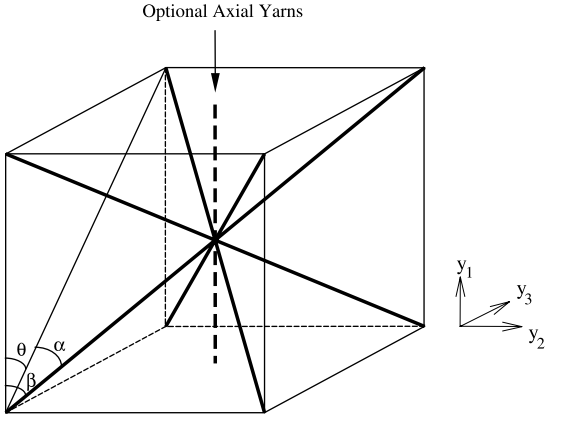

Fig. 1. Repetitive unit cell for a 3-D braided fabric.

3.1. Incompatible finite element

Based upon the general formulation of incompatible functions [23], the NH11 incompatible element is generated and adopted here. The incompatible parts of the displacement are hence introduced as follows:

$$\boldsymbol{u} = \boldsymbol{N}\boldsymbol{q} + \boldsymbol{N}^*\boldsymbol{\lambda} \tag{13}$$

where $\boldsymbol{N}^*$ is the shape functions of incompatible displacements of the element NH11. $\boldsymbol{\lambda}$ denotes the displacement parameters in the element. Once the geometric relation is introduced, there is

$$\boldsymbol{e} = (\boldsymbol{D}\boldsymbol{N})\boldsymbol{q} + (\boldsymbol{D}\boldsymbol{N}^*)\boldsymbol{\lambda} = \boldsymbol{B}\boldsymbol{q} + \overline{\boldsymbol{B}}\boldsymbol{\lambda} \tag{14}$$

where $\boldsymbol{D}$ denotes the differential operator in the relationship between the strain and displacement. Based on the potential principle of incompatible system, Eq. (12) can be written in the variational form:

$$\begin{aligned}\Pi_{\mathrm{p}} = \sum \Bigg[& \int_{V^{\mathrm{e}}} (\delta\boldsymbol{q}^{\mathrm{T}}\boldsymbol{B}^{\mathrm{T}} + \delta\boldsymbol{\lambda}^{\mathrm{T}}\overline{\boldsymbol{B}}^{\mathrm{T}})\boldsymbol{C}(\boldsymbol{B}\boldsymbol{q} + \overline{\boldsymbol{B}}\boldsymbol{\lambda})\,\mathrm{d}V \\ & + \int_{V^{\mathrm{e}}} (\delta\boldsymbol{q}^{\mathrm{T}}\boldsymbol{B}^{\mathrm{T}} + \delta\boldsymbol{\lambda}^{\mathrm{T}}\overline{\boldsymbol{B}}^{\mathrm{T}})\boldsymbol{C}\,\mathrm{d}V \Bigg]\end{aligned} \tag{15}$$

where V^{e} denotes the volume of every element in the domain Y. By using the extreme value condition, the following equations are derived:

$$\begin{aligned}&\left(\int_{V^{\mathrm{e}}} \boldsymbol{B}^{\mathrm{T}}\boldsymbol{C}\boldsymbol{B}\,\mathrm{d}V\right)\boldsymbol{q} + \left(\int_{V^{\mathrm{e}}} \boldsymbol{B}^{\mathrm{T}}\boldsymbol{C}\overline{\boldsymbol{B}}\,\mathrm{d}V\right)\boldsymbol{\lambda} = -\int_{V^{\mathrm{e}}} \boldsymbol{B}^{\mathrm{T}}\boldsymbol{C}\,\mathrm{d}V \\ &\left(\int_{V^{\mathrm{e}}} \overline{\boldsymbol{B}}^{\mathrm{T}}\boldsymbol{C}\boldsymbol{B}\,\mathrm{d}V\right)\boldsymbol{q} + \left(\int_{V^{\mathrm{e}}} \overline{\boldsymbol{B}}^{\mathrm{T}}\boldsymbol{C}\overline{\boldsymbol{B}}\,\mathrm{d}V\right)\boldsymbol{\lambda} = -\int_{V^{\mathrm{e}}} \overline{\boldsymbol{B}}^{\mathrm{T}}\boldsymbol{C}\,\mathrm{d}V\end{aligned} \tag{16}$$

It can be written in the form of matrix, i.e.,

$$\begin{bmatrix}\boldsymbol{K}_{qq} & \boldsymbol{K}_{q\lambda} \\ \boldsymbol{K}_{\lambda q} & \boldsymbol{K}_{\lambda\lambda}\end{bmatrix}\begin{Bmatrix}\boldsymbol{q} \\ \boldsymbol{\lambda}\end{Bmatrix} = \begin{bmatrix}\boldsymbol{P}_q \\ \boldsymbol{P}_\lambda\end{bmatrix} \tag{17}$$

From the second row of the above equation, $\boldsymbol{\lambda}$ can be expressed in terms of $\boldsymbol{q}$. Then, the stiffness equation of incompatible element is obtained:

$$(\boldsymbol{K}_{qq} - \boldsymbol{K}_{q\lambda}\boldsymbol{K}_{\lambda\lambda}^{-1}\boldsymbol{K}_{\lambda q})\boldsymbol{q} = \boldsymbol{P}_q - \boldsymbol{K}_{q\lambda}\boldsymbol{K}_{\lambda\lambda}^{-1}\boldsymbol{P}_\lambda \tag{18}$$

Considering that the equivalent nodal force of the element should not account for the effect of the incompatible shape function $\boldsymbol{N}^*$, the stiffness equation (18) is revised into

$$(\boldsymbol{K}_{qq} - \boldsymbol{K}_{q\lambda}\boldsymbol{K}_{\lambda\lambda}^{-1}\boldsymbol{K}_{\lambda q})\boldsymbol{q} = \boldsymbol{P}_q \tag{19}$$

3.2. Hybrid stress element

According to the Hellinger–Reissner variational principle, the energy functional of the incompatible discrete system can be expressed as

$$\begin{aligned}\Pi_{\mathrm{H\text{–}R}} = \sum \Bigg\{ \int_{V^{\mathrm{e}}} \Bigg[& -\frac{1}{2}\boldsymbol{\sigma}^{\mathrm{T}}\boldsymbol{S}\boldsymbol{\sigma} + \boldsymbol{\sigma}^{\mathrm{T}}(\boldsymbol{D}\boldsymbol{u}_q) \\ & + \boldsymbol{\sigma}_{\mathrm{h}}^{\mathrm{T}}(\boldsymbol{D}\boldsymbol{u}_\lambda) - \boldsymbol{f}(\boldsymbol{u}_q + \boldsymbol{u}_\lambda)\Bigg]\mathrm{d}V \Bigg\}\end{aligned} \tag{20}$$

where $\boldsymbol{S}$ is the compliance matrix of the element material. $\boldsymbol{u}_q$ and $\boldsymbol{u}_\lambda$ are the compatible and incompatible parts of the element displacement, respectively. $\boldsymbol{f}$ is the generalized body force that corresponds to the last term in Eq. (10). $\boldsymbol{\sigma}$ is the stress which can be assumed to be the sum of the constant stress $\boldsymbol{\sigma}_{\mathrm{c}}$ and the higher-order stress $\boldsymbol{\sigma}_{\mathrm{h}}$, i.e.,

$$\boldsymbol{\sigma} = \boldsymbol{\sigma}_{\mathrm{c}} + \boldsymbol{\sigma}_{\mathrm{h}} = \boldsymbol{\beta}_{\mathrm{c}} + \boldsymbol{\phi}_{\mathrm{h}}\boldsymbol{\beta}_{\mathrm{h}} = \boldsymbol{\beta}_{\mathrm{c}} + [\,\boldsymbol{\phi}_{\mathrm{I}} \quad \boldsymbol{\phi}_{\mathrm{II}}\,]\begin{Bmatrix}\boldsymbol{\beta}_{\mathrm{I}} \\ \boldsymbol{\beta}_{\mathrm{II}}\end{Bmatrix} \tag{21}$$

Based on the consistency requirement of incompatible hybrid element, the optimizing condition for hybrid element is applied [5], that is

$$\oint_{\partial V^{\mathrm{e}}} \delta\boldsymbol{u}_\lambda^{\mathrm{T}}\boldsymbol{n}\boldsymbol{\sigma}_{\mathrm{h}}\,\mathrm{d}S = 0 \tag{22}$$

where ∂V^{e} is the element boundary and $\boldsymbol{n}$ is the outward normal vector of the element boundary. Substituting the expressions (13) and (21) into (22) induces

$$\delta\boldsymbol{\lambda}^{\mathrm{T}}\boldsymbol{M}\boldsymbol{\beta}_{\mathrm{h}} = 0 \tag{23}$$

where

$$\boldsymbol{M} = \oint_{\partial V^{\mathrm{e}}} \boldsymbol{N}^{*\mathrm{T}}\boldsymbol{n}[\,\boldsymbol{\phi}_{\mathrm{I}} \quad \boldsymbol{\phi}_{\mathrm{II}}\,]\mathrm{d}S = [\,\boldsymbol{M}_{\mathrm{I}} \quad \boldsymbol{M}_{\mathrm{II}}\,] \tag{24}$$

and

$$\begin{aligned}\boldsymbol{M}_{\mathrm{I}} &= \int_{V^{\mathrm{e}}} [(\boldsymbol{D}\boldsymbol{N}^*)^{\mathrm{T}}\boldsymbol{\phi}_{\mathrm{I}} + \boldsymbol{N}^{*\mathrm{T}}(\boldsymbol{D}^{\mathrm{T}}\boldsymbol{\phi}_{\mathrm{I}})]\,\mathrm{d}V \\ \boldsymbol{M}_{\mathrm{II}} &= \int_{V^{\mathrm{e}}} [(\boldsymbol{D}\boldsymbol{N}^*)^{\mathrm{T}}\boldsymbol{\phi}_{\mathrm{II}} + \boldsymbol{N}^{*\mathrm{T}}(\boldsymbol{D}^{\mathrm{T}}\boldsymbol{\phi}_{\mathrm{II}})]\,\mathrm{d}V\end{aligned} \tag{25}$$

It is difficult to get the analytical form of $\boldsymbol{M}_{\mathrm{I}}$ and $\boldsymbol{M}_{\mathrm{II}}$. However they are functions of the nodal coordinates of the element and can be calculated by numerical integration. From Eq. (23), there is

$$[\,\boldsymbol{M}_{\mathrm{I}} \quad \boldsymbol{M}_{\mathrm{II}}\,]\begin{Bmatrix}\boldsymbol{\beta}_{\mathrm{I}} \\ \boldsymbol{\beta}_{\mathrm{II}}\end{Bmatrix} = 0 \tag{26}$$

Expressing $\boldsymbol{\beta}_{\mathrm{II}}$ in terms of $\boldsymbol{\beta}_{\mathrm{I}}$ leads to

$$\boldsymbol{\sigma} = \boldsymbol{\sigma}_{\mathrm{c}} + \boldsymbol{\sigma}_{\mathrm{h}} = \boldsymbol{\beta}_{\mathrm{c}} + \boldsymbol{\phi}_{\mathrm{h}}^*\boldsymbol{\beta}_{\mathrm{I}} \tag{27}$$

where

$$\boldsymbol{\phi}_{\mathrm{h}}^* = \boldsymbol{\phi}_{\mathrm{I}} - \boldsymbol{\phi}_{\mathrm{II}}\boldsymbol{M}_{\mathrm{II}}^{-1}\boldsymbol{M}_{\mathrm{I}} \tag{28}$$

Substituting Eq. (27) into (20), the Hellinger–Reissner variational principle is rewritten as

$$\Pi^{e}(\boldsymbol{\sigma}_c, \boldsymbol{\sigma}_h, \boldsymbol{u}_q, \boldsymbol{u}_\lambda) = \int_{V^e} \left[-\frac{1}{2}(\boldsymbol{\sigma}_c + \boldsymbol{\sigma}_h)^T \boldsymbol{S}(\boldsymbol{\sigma}_c + \boldsymbol{\sigma}_h) + (\boldsymbol{\sigma}_c + \boldsymbol{\sigma}_h)^T (\boldsymbol{D}\boldsymbol{u}_q) + \boldsymbol{\sigma}_h^T (\boldsymbol{D}\boldsymbol{u}_\lambda) - \boldsymbol{f}(\boldsymbol{u}_q + \boldsymbol{u}_\lambda) \right] dV \quad (29)$$

From the stagnation value condition of the functional (29), the stiffness equation of the hybrid element can be obtained.

4. Numerical evaluations and discussions

In this study, textile composites of four-step braiding process with a 1×1 pattern are used. A currently employed representative volume element (RVE) or unit cell [2,3] that captures the major features of the underlying microstructure and composition is shown in Fig. 1. The only two independent variables include the surface braid angle θ and the system fiber volume fraction v_f. Based on the typical geometric RVE, the isostrain and isostress mechanical models were first created to study its response under loading conditions [2,3].

In this section, the experimental results as well as the predictions from the isostrain model (ISN) and the weighted average model (WAM) are excerpted from [3], while the predictions from the isoparametric displacement element (ISO) detailed in [24], the incompatible displacement element (INC), and the hybrid stress element (HYB) are performed in this paper. Numerical results from the five approaches are compared with experimental measurements. Next, a parametric study using the hybrid stress element method is carried out to investigate the effects on the global effective mechanical properties of the independent system parameters of the 3-D braided composites.

4.1. Experimental data and comparisons

The braid threads are AS-4 yarn (6K) of graphite fiber by Hercules and the matrix is the Shell 862 epoxy resin with W curing agent. Their elastic properties are shown in Table 1. Table 2 summaries the details of the specimens tested experimentally in [3]. Tables 3 and 4 present a comparison of the experimental measurements against the predictions from the five different models including both predictions and associated percentage errors. The tolerance in measured values is within ±8.5%.

It can be shown that the errors of the five analytical methods are all reasonably small for the unidirectional samples. There are however differences between the predictions in the case of 3-D braided samples. When there is no axial yarn, the three models ISO, WAM and HYB predict results closer to experimental measurements than both ISN and INC. Furthermore, it is shown that the HYB model generates an overall more stable error level. Even in the case where axial yarn is used, the HYB model still gives acceptable prediction. Similar conclusion can be reached from the comparison of results of the transverse moduli in Table 4. So in general, the HYB method can give more accurate and stable numerical results for a wide range of braided composites, compared to the experimental results.

4.2. A parametric study on the effective mechanical properties

Using the hybrid finite element method, the effective mechanical properties of 3-D composites by four-step

Table 1
Elastic properties of epoxy resin and AS-4 yarns [3]

Epoxy resin		AS-4 yarns				
E (GPa)	G (GPa)	E_{f1} (GPa)	E_{f2} (GPa)	G_{f12} (GPa)	G_{f23} (GPa)	v_{f12}
2.94	1.07	234.6	13.8	13.8	5.5	0.2

Table 2
Details of the specimen geometric parameters [3]

Sample ID	Architecture	θ	v_f
U1	Unidirectional	0	0.27
U2	Unidirectional	0	0.28
U3	Unidirectional	0	0.23
B1	Braided	17	0.38
B2	Braided	17	0.40
B3	Braided	20	0.46
B4	Braided	22	0.44
B5	Braided	25	0.29
BA1	Braided with axials	0, 25	0.53 (28% axials)

Table 3
Comparison of measured and predicted longitudinal moduli for the various composites considered in this study

Sample ID	Measure (GPa)	ISN		WAM		ISO		INC		HYB	
		(GPa)	(%)	(GPa)	(%)	(GPa)	(%)	(GPa)	(%)	(GPa)	(%)
U1	62.6	65.5	4.6	65.5	4.6	63.6	1.6	63.6	1.6	63.6	1.6
U2	66.9	68.8	2.8	68.8	2.8	69.2	3.4	69.2	3.4	69.2	3.4
B1	43.6 ± 1.9	55.7	27.8	48.3	10.8	39.3	9.9	32.5	25.5	46.0	5.5
B2	45.9 ± 1.2	58.4	27.2	50.7	10.5	40.4	12.0	33.4	27.2	46.9	2.2
B3	48.0 ± 3.0	53.7	11.9	47.0	2.1	40.1	16.5	33.2	30.8	44.8	6.7
B4	38.5 ± 2.4	43.7	13.5	38.6	0.3	34.5	10.4	28.6	25.7	38.1	1.0
B5	21.2 ± 1.8	23.8	12.3	21.4	0.9	21.2	0.0	17.1	19.3	23.8	12.3
BA1	59.2 ± 1.2	65.8	11.2	56.8	4.1	49.0	17.2	44.3	25.2	54.8	7.4

Table 4
Comparison of measured and predicted transverse moduli for the various composites considered in this study

Sample ID	Measure (GPa)	ISN		WAM		ISO		INC		HYB	
		(GPa)	(%)	(GPa)	(%)	(GPa)	(%)	(GPa)	(%)	(GPa)	(%)
U3	5.52	4.79	13.22	4.79	13.22	5.01	9.24	4.87	11.78	4.98	9.78
B1	6.21 ± 0.41	5.74	7.57	5.74	7.57	6.17	0.64	5.67	8.70	6.22	0.16
B4	6.02 ± 0.30	6.22	3.32	6.21	3.16	6.56	8.97	6.15	2.16	6.54	8.64

1×1 braiding process have been predicted as shown in Figs. 2–9 where *ag15*, *ag25* and *ag25a* denote the surface braid angle $\theta = 15°$, 25°, and 25° with 30% axial yarns, and v_f40, v_f50 and v_f50a are the fiber volume fraction $v_f = 40\%$, 50%, and 50% with 36% axial yarns, respectively.

In Figs. 2 and 3, with an increase in surface braid angle, the system longitudinal modulus decreases at a given fiber volume fraction. If there are lay-ins of axial yarns however, the loss in longitudinal modulus can be significantly reduced. As expected, the longitudinal modulus increases with the fiber volume fraction. In Figs. 4 and 5 of transverse modulus, the modulus augments with an increase in either surface braid angle or the fiber volume fraction. The existence of axial yarn

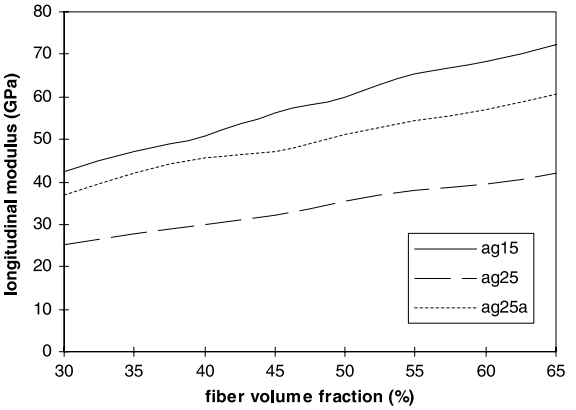

Fig. 3. Longitudinal modulus versus fiber volume fraction.

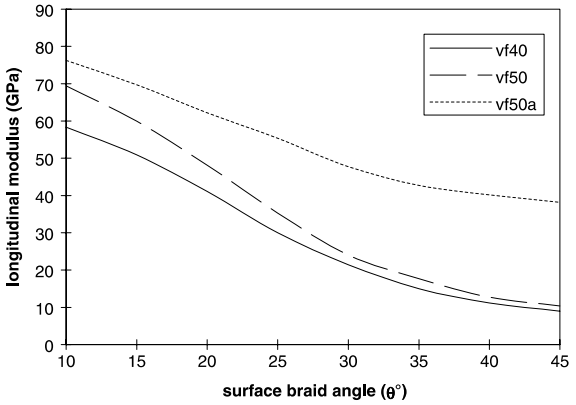

Fig. 2. Longitudinal modulus versus surface braid angle.

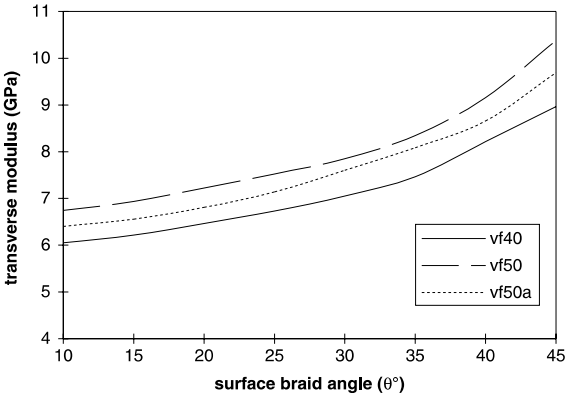

Fig. 4. Transverse modulus versus surface braid angle.

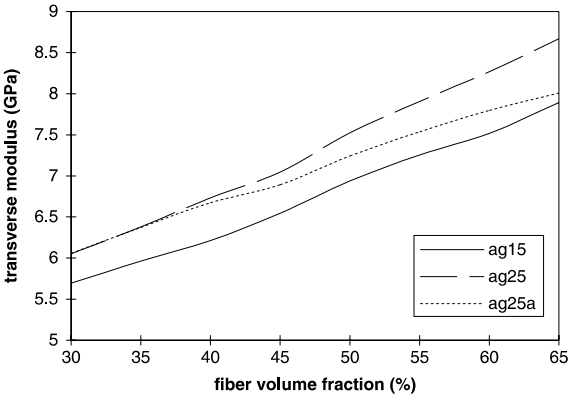

Fig. 5. Transverse modulus versus fiber volume fraction.

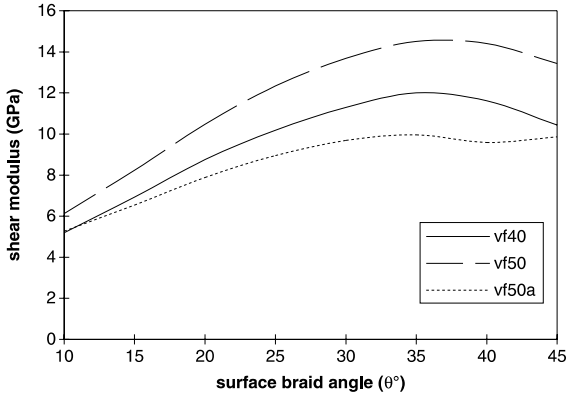

Fig. 6. Shear modulus versus surface braid angle.

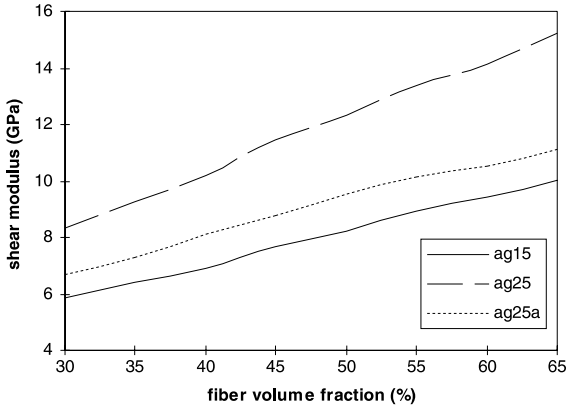

Fig. 7. Shear modulus versus fiber volume fraction.

leads to a slightly lower modulus. The variations of the shear modulus with the surface braid angle and fiber fraction are depicted in Figs. 6 and 7. Notice that in Fig. 6 there is an optimal value for the surface braid angle

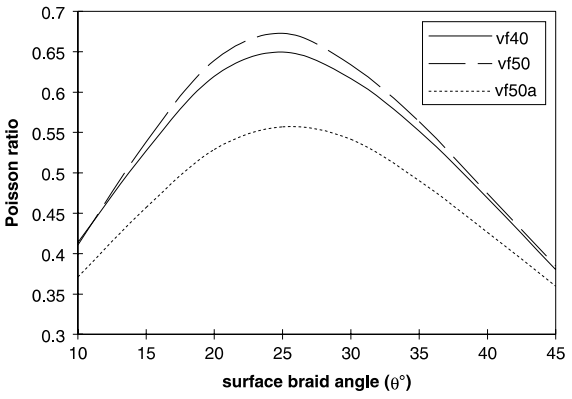

Fig. 8. Poisson's ratio versus surface braid angle.

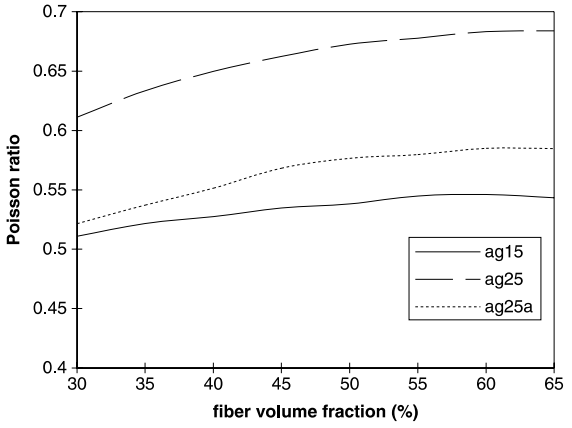

Fig. 9. Poisson's ratio versus fiber volume fraction.

where the shear modulus reaches the maximum; yet the axial yarn seemly diminishes this characteristic. Again the shear modulus increases as fiber fraction increases. This phenomenon of optimal surface braid angle shows more significantly in the case of major Poisson's ratio shown in Fig. 8, even when the axial yarn is used. The axial yarn has a distinctive effect on Poisson's ratio at given θ and v_f values, and likewise, a greater v_f leads to a higher Poisson's ratio (Fig. 9).

5. Conclusions

Incorporating with homogenization method, both the incompatible displacement element and hybrid stress element are developed to predict the mechanical behavior of braided composites. The incompatible element in this paper can pass the patch test condition. The hybrid element is constructed based upon the consistency condition.

The hybrid element method provides the best results comparing to the experimental measurements in the

micromechanics of 3-D braided composites, among all five methods considered here including the incompatible element approach.

A parametric study using the homogenization theory combined with the hybrid stress element is conducted for system effective mechanical properties of 3-D braided composites. It provides a robust design guide for 3-D braided composite materials.

Acknowledgements

The authors gratefully wish to acknowledge the financial support by Australian Research Council and by National Natural Science Foundation of China under grant no. 19702016.

References

[1] Shackelford JF. Introduction to materials science for engineers. Upper Saddle River, NJ: Prentice-Hall; 1996.
[2] Yang JM, Ma CL, Chou TW. Fiber inclination model of three-dimensional textile structural composites. J Compos Mater 1986;20(9):472–84.
[3] Kalidindi SR, Abusafieh A. Longitudinal and transverse moduli and strengths of low angle 3-D braided composites. J Compos Mater 1996;30(8):885–905.
[4] Pian THH. Derivation of element stiffness matrices by assumed stress distributions. AIAA J 1964;2:1333–6.
[5] Wu CC, Bufler H. Multivariable finite elements: consistency and optimization. Sci China (A) 1991;34:284–99.
[6] Wu CC, Pian THH. Incompatible numerical analysis and hybrid element method. Beijing: Science Press; 1997.
[7] Bensoussan A, Lions JL, Papanicolaou G. Asymptotic analysis for periodic structures. New York: North-Holland Publishing Company; 1978.
[8] Sanchez-Palencia E, Zaoui A. Homogenization techniques for composite media. New York: Springer-Verlag; 1987.
[9] Kalamkarov AL. Composite and reinforced elements of construction. New York: Wiley; 1992.
[10] Lukkassen D, Persson LE, Wall P. Some engineering and mathematical aspects on the homogenization method. Compos Part B: Engrg 1995;5:519–31.
[11] Lin CC, Segel LA. Mathematics applied to deterministic problems in the natural sciences. Philadelphia, PA: SIAM; 1988.
[12] Fish J, Nayak P, Holmes MH. Microscale reduction error indicators and estimators for a periodic heterogeneous medium. Comput Mech 1994;14:323–38.
[13] Wentorf R, Collar R, Shephard MS, Fish J. Automated modeling for complex woven mesostructures. Comput Methods Appl Mech Engrg 1999;172:273–91.
[14] Fish J, Shek K. Multiscale analysis of composite materials and structures. Compos Sci Technol 2000;60(12–13):2547–56.
[15] Ghosh S, Lee K, Raghavan P. A multi-level computational model for multi-scale damage analysis in composite and porous materials. Int J Solids and Structures 2001;38(14):2335–85.
[16] Ghosh S, Lee K, Moorthy S. Multiple scale analysis of heterogeneous elastic structures using homogenization theory and voronoi cell finite element method. Int J Solids and Structures 1995;32(1):27–62.
[17] Guedes JS, Kikuchi N. Preprocessing and postprocessing for materials based on the homogenization method with adaptive finite element methods. Comput Methods Appl Mech Engrg 1989;83:143–98.
[18] Hollister SJ, Kikuchi N. A comparison of homogenization and standard mechanics analyses for periodic porous composites. Comput Mech 1992;10:73–95.
[19] Lissenden CJ, Herakovich CT. Numerical modeling of damage development and viscoplasticity in metal matrix composites. Comput Methods Appl Mech Engrg 1995;126(3–4):289–303.
[20] Karihaloo BL, Xiao QZ, Wu CC. Homogenization-based multivariable element method for pure torsion of composite shafts. Comput & Structures 2001;79(18):1645–60.
[21] Lene F, Leguillon D. Homogenized constitutive law for a partially cohesive composite material. Int J Solids and Structures 1982;18:443–58.
[22] Jansson S. Homogenized nonlinear constitutive properties and local stress concentrations for composites with periodic internal structure. Int J Solids and Structures 1992;29:2181–200.
[23] Wu CC, Huang MG, Pian THH. Consistency condition and convergence criteria of incompatible elements: General formulation of incompatible functions and its application. Comput & Structures 1987;27:639–44.
[24] Bathe KJ. Finite element procedures in engineering analysis. Englewood Cliffs, NJ: Prentice-Hall; 1982.